Widely Used Variants of the Farquhar-von-Caemmerer-Berry Model Can Cause Errors in Parameter Estimation

Edward B. Lochocki[1] and Justin M. McGrath[1,2,3*]

[1]Carl R. Woese Institute for Genomic Biology, University of Illinois, Urbana–Champaign, Urbana, IL, USA

[2]Plant Biology Department, University of Illinois, Urbana–Champaign, Urbana, IL, USA

[3]USDA ARS Global Change and Photosynthesis Research Unit, Urbana, IL, USA

*Corresponding author's email address: justin.mcgrath@usda.gov

CENTRAL THEME OF THE MANUSCRIPT: The Farquhar-von-Caemmerer-Berry model of CO_2 assimilation plays a key role in plant research, but many publications use variants of the model that differ from the original and can potentially introduce errors in photosynthetic parameter estimates.

NOVEL RESULTS, IDEAS, OR METHODS: Using a literature survey, FvCB model variants are categorized, and some are found to make contradictory predictions. Comparisons against A-C_i curves show that the "min-W variant" exhibits the best performance, especially at low CO_2 concentrations.

ABSTRACT: The Farquhar-von-Caemmerer-Berry (FvCB) model is the most widely-used mechanistic model of C_3 net CO_2 assimilation, and it plays a significant role in plant physiology, ecology, climate science, and Earth system modeling. As use of the model has grown, multiple variants have appeared across publications. Although many of these are commonly used, there has not been a detailed investigation of existing variants and their impacts on results and interpretations. Here we summarize the types of variants and their prevalence in the literature, and we present a comprehensive comparison of differences between them. A key finding is that a common variant that uses the minimum of assimilation rates rather than the minimum of

carboxylation rates, which we call the "min-*A* variant," makes different predictions than the original "min-*W* variant," yet appears in approximately half of highly-cited publications and software tools that use the FvCB model. Another concern is that although leaf biochemistry restricts the range of CO_2 partial pressures where limitations due to triose phosphate utilization (TPU) can occur, this restriction is commonly omitted from the model's equations. Among other potential issues, these variations can introduce errors exceeding 20% when estimating photosynthetic parameter values from CO_2 response curves. It is therefore important to be aware of this source of error when fitting the model, to avoid using the min-*A* variant, and to include the biochemically-derived CO_2 threshold for TPU limitations.

KEYWORDS: Fitting A-C_i curves, photosynthesis at low CO_2 concentrations, triose phosphate utilization (TPU), ribulose 1,5-bisphosphate (RuBP) depletion, estimating $V_{c,max}$

1. INTRODUCTION

The Farquhar-von-Caemmerer-Berry (FvCB) model for C_3 net CO_2 assimilation is a cornerstone of modern plant biology, ecology, and climate science, having been highly successful in explaining experimental measurements and making predictions at scales ranging from single cells to the entire globe (Farquhar et al., 2001; Von Caemmerer, 2013). Although commonly referred to by the names of the authors of a key 1980 publication (Farquhar et al., 1980), the FvCB model is nonetheless built on decades of research that predates 1980, and it has been improved by other researchers since its initial description (Yin et al., 2021). It is a mechanistic model based on a simplified version of the light-dependent reactions, the Calvin-Benson-Bassham (CBB) cycle, and the photorespiratory cycle, and it consists of a small set of equations for predicting net CO_2 assimilation rates (Farquhar et al., 1980; Farquhar and von Caemmerer, 1982; Kirschbaum and Farquhar, 1984). In a plant physiology context, the many possible applications of the FvCB model include assessing the impact of elevated atmospheric CO_2 concentrations on photosynthesis (Bernacchi et al., 2005), identifying limitations to photosynthetic CO_2 assimilation (Busch and Sage, 2017), evaluating the genetic diversity of ribulose-1,5-bisphosphate carboxylase-oxygenase (Rubisco) carboxylation efficiency within a species (De Souza et al., 2020), and helping to guide strategies for developing sustainable and

high-performing crops in the face of climate change (He and Matthews, 2023; Matthews et al., 2022; Wu et al., 2023; Yin and Struik, 2017).

The FvCB model works by separately calculating three potential rates of ribulose 1,5-bisphosphate (RuBP) carboxylation as catalyzed by Rubisco, which are limited by either Rubisco activity (W_c), RuBP regeneration (W_j), or triose phosphate utilization (TPU) (W_p). The slowest potential rate is chosen as the actual RuBP carboxylation rate (V_c). The net leaf-level CO_2 assimilation rate (A_n) can then be determined by subtracting CO_2 losses due to RuBP oxygenation and non-photorespiratory CO_2 release from the gains due to RuBP carboxylation. Mathematically, this process can be expressed by five equations:

$$W_c = \frac{C \cdot V_{c,max}}{C + K_c \cdot \left(1 + \frac{O}{K_o}\right)} \tag{1a}$$

$$W_j = \frac{C \cdot J}{4 \cdot C + 8 \cdot \Gamma^*} \tag{1b}$$

$$W_p = \begin{cases} \infty, & C \leq \Gamma^* \cdot (1 + 3 \cdot \alpha_{old}) \\ \frac{3 \cdot C \cdot T_p}{C - \Gamma^* \cdot (1 + 3 \cdot \alpha_{old})}, & C > \Gamma^* \cdot (1 + 3 \cdot \alpha_{old}) \end{cases} \tag{1c}$$

$$V_c = \min\{W_c, W_j, W_p\} \tag{1d}$$

$$A_n = V_c \cdot \left(1 - \frac{\Gamma^*}{C}\right) - R_L \tag{1e}$$

Here, C is the partial pressure of CO_2 in the vicinity of Rubisco. Definitions for all the symbols used in these equations can be found in Table **1**. Although Equation **1** differs from early expressions of the FvCB model in its approach to TPU limitations (Farquhar and von Caemmerer, 1982; Kirschbaum and Farquhar, 1984), it follows the original reasoning for identifying the rate-limiting process, which we refer to as the "min-*W* approach."

Symbol	**Meaning**	**Units**	**Range**	**Typical value**
A_n	Net CO_2 assimilation rate	μmol m^{-2} s^{-1}	-	-

A_c	Net CO_2 assimilation rate when RuBP carboxylation is limited by Rubisco activity	μmol m^{-2} s^{-1}	-	-
$A_c\|_{C=0}$	The value of A_c when C = 0	μmol m^{-2} s^{-1}	-	-
A_d	Net CO_2 assimilation rate when RuBP carboxylation is limited by substantial Rubisco deactivation or RuBP depletion at low C	μmol m^{-2} s^{-1}	-	-
A_j	Net CO_2 assimilation rate when RuBP carboxylation is limited by the rate of electron transport going to support RuBP regeneration[(b)]	μmol m^{-2} s^{-1}	-	-
$A_j\|_{C=0}$	The value of A_j when C = 0	μmol m^{-2} s^{-1}	-	-
A_p	Net CO_2 assimilation rate when RuBP carboxylation is limited by the rate of inorganic phosphate release from TPU	μmol m^{-2} s^{-1}	-	-
C	Partial pressure of CO_2 in the vicinity of Rubisco	μbar	$0 \leq C$	-
C_{cj}	The value of C where W_c = W_j	μbar	$0 \leq C_{cj}$	-
C_c	Chloroplastic partial pressure of CO_2	μbar	$0 \leq C_c$	-
C_i	Intercellular partial pressure of CO_2	μbar	$0 \leq C_i$	-
C_i^*	The value of C_i when $C_c = \Gamma^*$	μbar	$0 \leq C_i^*$	-
J	Potential rate of electron transport going to support RuBP regeneration at a given light intensity	μmol m^{-2} s^{-1}	$0 \leq J$	170[(a)]
J_{eq}	The value of J where $A_c\|_{C=0}$ = $A_j\|_{C=0}$	μmol m^{-2} s^{-1}	$0 \leq J_{eq}$	-
J_d	The value of J where the denominator of Supplemental Equation **A5** is zero	μmol m^{-2} s^{-1}	$0 \leq J_d$	-
J_n	The value of J where the numerator of Supplemental Equation **A5** is zero	μmol m^{-2} s^{-1}	$0 \leq J_n$	-
K_c	Michaelis-Menten constant for CO_2	μbar	$0 < K_c$	259[(a)]
K_o	Michaelis-Menten constant for O_2	mbar	$0 < K_o$	179[(a)]
O	Partial pressure of O_2 in the vicinity of Rubisco	mbar	$0 \leq O$	210
Q_{in}	Incident photosynthetically active flux density	μmol m^{-2} s^{-1}	$0 \leq Q_{in}$	-
R_L	Rate of non-photorespiratory CO_2 release in the light	μmol m^{-2} s^{-1}	$0 \leq R_L$	1[(a)]

R_{pc}	Net rate of inorganic phosphate consumption in the chloroplast due to photosynthesis and photorespiration[(c)]	µmol m^{-2} s^{-1}	-	-
T_p	Potential rate of TPU	µmol m^{-2} s^{-1}	$0 < T_p$	11.8[(a)]
V_c	RuBP carboxylation rate	µmol m^{-2} s^{-1}	$0 \leq V_c$	-
$V_{c,max}$	Maximum rate of Rubisco carboxylation activity	µmol m^{-2} s^{-1}	$0 \leq V_{c,max}$	100[(a)]
V_o	RuBP oxygenation rate	µmol m^{-2} s^{-1}	$0 \leq V_o$	-
W_c	RuBP carboxylation rate limited by Rubisco activity	µmol m^{-2} s^{-1}	$0 \leq W_c$	-
W_d	RuBP carboxylation rate limited by substantial Rubisco deactivation or RuBP depletion at low C	µmol m^{-2} s^{-1}	$0 \leq W_d$	0
W_j	RuBP carboxylation rate limited by the rate of electron transport going to support RuBP regeneration[(b)]	µmol m^{-2} s^{-1}	$0 \leq W_j$	-
W_p	RuBP carboxylation rate limited by the rate of inorganic phosphate release from TPU	µmol m^{-2} s^{-1}	$0 \leq W_p$	-
α_{old}	Fraction of remaining glycolate carbon not returned to the chloroplast after accounting for carbon released as CO_2[(d)]	dimensionless	$0 \leq \alpha_{old} \leq 1$	0[(a)]
α_G	Fraction of glycolate carbon exported from the photorespiratory pathway as glycine	dimensionless	$0 \leq \alpha_G \leq 1$	0
α_S	Fraction of glycolate carbon exported from the photorespiratory pathway as serine	dimensionless	$0 \leq \alpha_S \leq \frac{3}{4}$	0
α_T	Fraction of glycolate carbon exported from the photorespiratory pathway as CH_2-THF	dimensionless	$0 \leq \alpha_T \leq \frac{1}{2}$	0
Γ^*	CO_2 compensation point in the absence of non-photorespiratory CO_2 release	µbar	$0 < \Gamma^*$	38.6[(a)]
Δ_c	Net rate of carbon production during the reduction of PGA to unbound RuBP	µmol m^{-2} s^{-1}	-	-

Table 1: Description of symbols used in this publication. Values marked with a superscript (a) are from the caption of Figure 2.6 in von Caemmerer (2000). The typical value for O in the table is the atmospheric value at sea level rounded to two significant figures. (b) By convention, the term "RuBP regeneration limitations" refers to the case where RuBP regeneration is limited primarily by electron transport, and possibly co-limited by the activity of CBB cycle enzymes such as sedoheptulose-1,7 bisphosphatase; limitations to RuBP regeneration imposed by the supply of inorganic phosphate or carbon are treated separately. (c) Consumption refers to the incorporation of inorganic phosphate into organic molecules. (d) Even when α_{old} is

zero, one quarter of glycolate carbon is released as CO_2 during glycine decarboxylation (Harley and Sharkey, 1991), so the overall fraction of glycolate carbon not returned to the chloroplast is $(1 + 3 \cdot \alpha_{old})/4$.

The conditional form of Equation **1c** ensures that $W_p \geq 0$ (as is necessary for a carboxylation rate) and that TPU cannot impose a limit on V_c when $C \leq \Gamma^* \cdot (1 + 3 \cdot \alpha_{old})$. This lower C threshold for TPU limitations will be discussed later in more detail. Note that a more complex version of the model separately includes glycolate carbon leaving the photorespiratory pathway as glycine, serine, or 5,10-methylene-tetrahydrofolate (CH_2-THF), requiring three α parameters instead of one: α_G, α_S, and α_T (Busch, 2020; Busch et al., 2018). Using the α_{old} model provides simplicity as it has fewer parameters, and thus it can more easily be applied. However, the biochemical basis for the three α version is better established, and it would be appropriate when the detail is necessary and the additional parameter values can be estimated. Here, we use the simpler α_{old} version for simplicity when comparing the other variants because the Busch *et al*. updates do not affect the general conclusions presented here (Supplemental Section **S1.2**).

Most applications of the FvCB model in scientific research require knowledge of the values of key parameters such as $V_{c,max}$, J, and T_p; for example, parameter values may be used to characterize groups of plants or as inputs to computational models. These parameter values can be estimated from experimentally measured CO_2 response curves, which are obtained by using a gas exchange system to record A_n and C_i as the CO_2 concentration around a leaf is varied under otherwise constant conditions of incident light, humidity, and temperature. By comparing the measured curve against predictions from the FvCB model made using $C = C_i$ or, if possible, $C = C_c$, it is possible to find values of the model parameters that best reproduce the measured assimilation rates. Many approaches to curve fitting can be found in the literature, some of which include additional types of data that can be used to estimate C_c, such as chlorophyll fluorescence (Bellasio et al., 2016; Duursma, 2015; Gu et al., 2010; Lochocki et al., 2025, 2025; Moualeu-Ngangue et al., 2017; Sharkey et al., 2007; Stinziano et al., 2021; Wang et al., 2017; Xiao et al., 2021).

As usage of the model for curve fitting and other purposes has increased, numerous additions and changes have occurred across scientific publications and software tools. Although many

researchers are familiar with the uses and drawbacks of these variants, a detailed comparison would be valuable for those learning about the model, with the aim of providing insight into which variants may be appropriate for particular scenarios. Here we summarize FvCB model variants and key differences between them (Table **2** and Supplemental Section **S1**). In some cases, the choice of a variant may depend on the situation, but we also demonstrate that some variants provide no benefits and can produce results that contradict measurements. One such group of variants replaces Equations **1d** and **1e** by a single equation calculating A_n as the minimum of three potential net assimilation rates (Figure **1a**). As described in detail below, this approach, which we refer to as the "min-*A* approach," alters the model's predictions for A_n when $C < \Gamma^*$ such that they disagree with measurements. Another issue is that although TPU limitations are understood to only occur at high C (Harley and Sharkey, 1991; Sharkey, 2019; Sharkey et al., 2007), the explicit lower C threshold for TPU included in Equation **1c** is often omitted, leading to situations where the model incorrectly predicts TPU to be limiting. The prevalence of these model variations in the literature and the potential consequences of using them in parameter estimates have not been explored.

Category	Approach	Abbreviation
Treatment of carbon leaving the photorespiratory pathway	Not considered	0-α
	α_{old}	1-α
	α_G and α_S	2-α
	α_G, α_S, and α_T	3-α
CO_2 threshold for TPU limitations	No TPU limitations	NT
	No explicit TPU threshold	NTT
	Fixed TPU threshold	FTT
	Biochemically-derived TPU threshold	BTT
Choice of limiting process	Minimum potential carboxylation rate	min-*W*
	Minimum potential net CO_2 assimilation rate	min-*A*
Additional constraints on choice of limiting process	No forced limitations	NFL
	Rubisco limitations forced at low CO_2	FRL

Table 2: Classification scheme for FvCB model equations or computer code. To fully describe a variant, its approach in each category must be specified; for example, 0-α+NT+min-A+NFL is a variant with no α parameters or TPU limitations where the limiting process is chosen using the min-A approach without any other constraints. Note that not all combinations are possible, and that some are special cases of others; for example, 0-α and 1-α are equivalent when α_{old} is zero.

While it is difficult or impossible to determine how often researchers use a particular variant, estimates can be made by surveying peer-reviewed publications (Supplemental Section **S2**). The min-*A* approach first appears in the literature around 1990, with Collatz et al. (1990) and Collatz et al. (1991) being the earliest examples found in the survey. Out of the highest-cited papers published since 1990 that discuss the FvCB model equations, slightly more than half use the min-*A* approach (Figure **1b**). The min-*A* approach was identified as an "incorrect form" of the FvCB model in a 2010 publication (Gu et al., 2010), but its problems were not explained or demonstrated, and thus highly-cited publications have continued to use it with roughly the same frequency since 2013 (Figure **1b**). Likewise, the min-*A* approach is more likely to be used in popular software tools for estimating FvCB model parameters from CO_2 response curves (Figure **1b**). Among the publications identified in this survey, only two include an explicit lower C threshold for TPU limitations: Gu et al. (2010) and Lochocki et al. (2025).

The survey of software tools also reveals the presence of two additional variations, which we refer to as the "forced Rubisco limitation" (FRL) and "fixed TPU threshold" (FTT) modifications (Table **2**). The FRL modification enforces Rubisco limitations at low C such that $A_n = A_c$ for $C \leq \Gamma^*$. The FTT modification prevents TPU limitations for C below a fixed threshold value, rather than the one in Equation **1c**, which is determined from leaf biochemistry. These modifications address some, but not all, biological and numerical issues related to other variants of the FvCB model equations, as described below.

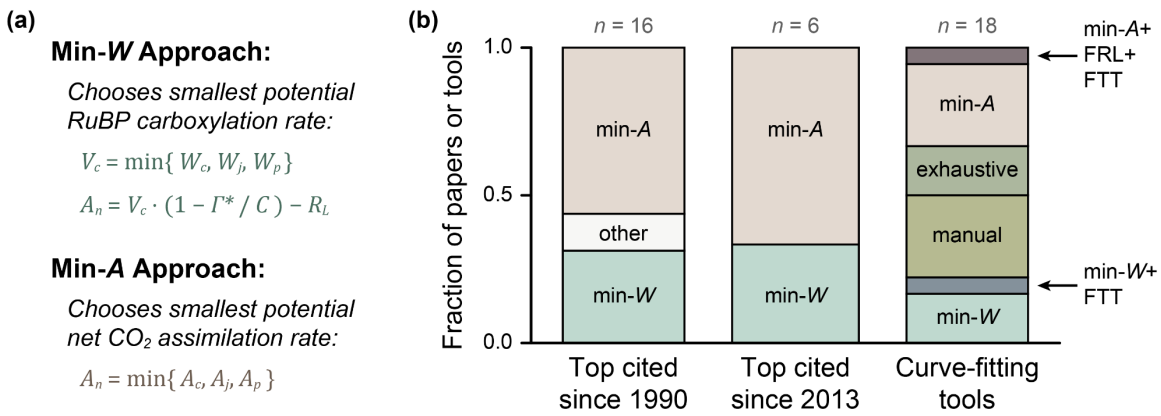

*Figure **1**: Description of the min-W and min-A approaches, and an estimate of their relative prevalence in the scientific literature. (**a**) Overview of the essential difference between the min-W and min-A approaches. The carboxylation rates W_c, W_j, and W_p that appear in the min-W approach can be calculated using Equation **1**, while the assimilation rates A_c, A_j, and A_p that appear in the min-A approach can be calculated using Equation **2**. (**b**) Fraction of highly cited papers (or tools for estimating FvCB model parameter values from CO_2 response curves) that use the min-W approach, the min-A approach, or other approaches (Supplemental Section **S2**).*

Although the literature survey presented here is limited (and does not include any software tools used in climate or agricultural modeling), it strongly suggests that many researchers working with biochemical models of C_3 net CO_2 assimilation have seen or used the min-*A* approach rather than the original min-*W* approach. It may even be possible that the min-*A* approach is more prevalent overall. Many researchers may also be unaware of the lower C threshold for TPU limitations. Given the central role of the FvCB model in several fields, it is necessary to elucidate the differences between the min-*W* and min-*A* approaches (with or without the FRL and FTT modifications) and to quantify the errors resulting from use of the min-*A* approach to estimate photosynthetic parameter values.

It might be argued that the differences between the min-*W* and min-*A* approaches are immaterial because all variants are incorrect when $C < \Gamma^*$ due to Rubisco deactivation and RuBP depletion, processes that are not explicitly included in the FvCB model. Based on this reasoning, some researchers may intentionally avoid making gas exchange measurements or performing curve fits at low C. Yet, the ability to fit CO_2 response curves for $C < \Gamma^*$ has not been systematically tested. Thus, there is an opportunity to better understand net CO_2 assimilation at low C by first expanding the FvCB model to include Rubisco deactivation and

RuBP depletion and then comparing the min-*W* and min-*A* approaches against measured assimilation rates for $C < \Gamma^*$.

The objectives of this study are to (1) describe the key differences between FvCB model variants, (2) establish the biochemical basis of the lower C threshold for TPU, (3) develop a simple way to include Rubisco deactivation and RuBP depletion in the FvCB framework, and (4) test the validity of the min-*W* and min-*A* approaches by fitting CO_2 response curves that extend to $C < \Gamma^*$. Our findings indicate that the min-*A* approach produces predictions that contradict observations, that the unrealistic predictions of the min-*A* approach cannot be fixed through the FRL and FTT modifications, and that the min-*A* approach cannot be extended to include Rubisco deactivation or RuBP depletion. In particular, the curve fits show that the min-*W* approach is able to represent C_3 net CO_2 assimilation at low C while the min-*A* approach cannot, leading to underestimates of V_{cmax} and J by up to 23% and 12%, respectively. Although errors are unlikely to be as severe in most situations, the min-*A* approach did not provide better predictions in any situation.

2. Description

2.1. The Min-W Variant

We categorize variations in FvCB model equations along several dimensions, such as the method used to determine the rate-limiting process, or the treatment of glycolate carbon leaving the photorespiratory pathway (Table **2**). Each dimension has several possible approaches, and each combination of possible approaches defines a variant. Equation **1** uses one α parameter (1-α), chooses a minimal carboxylation rate (min-*W*), uses the biochemically derived threshold for TPU limitations (BTT), and does not force Rubisco limitations at low C (NFL). Thus, it would be described as the 1-α+BTT+min-*W*+NFL variant. We refer to it as "the min-W variant" for brevity, since it is a representative example of the broader group of variants that use the min-*W* approach.

Here we note that within the time scale of a typical gas exchange measurement, the main environmental influences on the potential carboxylation rates are C, Q_{in}, O, and temperature.

Note that some of this influence is not immediately obvious; for example, Γ^* depends on O, and J depends on Q_{in} and other factors (von Caemmerer, 2000). For simplicity, we assume constant temperature and treat Γ^* and J as inputs to the model, especially since several different approaches are available for calculating J from Q_{in} (Walker et al., 2021). As C, J, and O vary, the slowest carboxylation rate may change. Changes in the rate-limiting process as C increases from zero will be discussed later in more detail (Section **3.2**).

2.2. The Min-A Variant

When RuBP carboxylation is Rubisco-limited, the corresponding net assimilation rate (called A_c rather than A_n to indicate the rate-limiting process) can be found by setting $V_c = W_c$ in Equation **1e** and replacing it with the expression in Equation **1a**:

$$A_c = W_c \cdot \left(1 - \frac{\Gamma^*}{C}\right) - R_L = \frac{(C-\Gamma^*)\cdot V_{c,max}}{C + K_C \cdot \left(1 + \frac{O}{K_O}\right)} - R_L. \tag{2a}$$

Likewise, when RuBP carboxylation is limited by RuBP regeneration or TPU, the corresponding net assimilation rates are given by analogous equations:

$$A_j = W_j \cdot \left(1 - \frac{\Gamma^*}{C}\right) - R_L = \frac{(C-\Gamma^*)\cdot J}{4\cdot C + 8\cdot \Gamma^*} - R_L, \tag{2b}$$

$$A_p = W_p \cdot \left(1 - \frac{\Gamma^*}{C}\right) - R_L = \frac{3\cdot (C-\Gamma^*)\cdot T_p}{C - \Gamma^* \cdot (1 + 3\cdot \alpha_{old})} - R_L. \tag{2c}$$

In the min-*A* approach, A_c, A_j, and A_p are considered to be potential net CO_2 assimilation rates and the actual net CO_2 assimilation rate is calculated as the smallest of the three, in analogy with Equations **1d** and **1e** from the min-*W* variant:

$$A_n = \min\{A_c, A_j, A_p\}. \tag{2d}$$

Specifically, Equation **2** describes the 1-α+NTT+min-*A*+NFL variant; we refer to this as the "min-*A* variant" for brevity, since it is a representative example of the broader group of variants that use the min-*A* approach.

Thus, the essential difference between Equations **1** and **2** is that the min-*W* variant chooses a minimal potential carboxylation rate, while the min-*A* variant chooses a minimal potential net

CO_2 assimilation rate (Figure **1a**). Another difference is that Equation **1c** restricts TPU limitations to $C > \Gamma^* \cdot (1 + 3 \cdot \alpha_{old})$, while Equation **2c** makes no such restriction. Many sources presenting the min-*W* approach also omit this restriction. Nevertheless, unreasonable results such as negative carboxylation rates and divergent behavior can occur in either variant when this restriction is not included; these issues have been noticed before and the FTT modification has been used to address them, although some issues remain when using a fixed TPU threshold (Section **3.3**).

3. Results

3.1. Minimal Carboxylation Rates Are Not Equivalent to Minimal Assimilation Rates

There are two irreconcilable differences between the min-*W* and min-*A* variants (Figure **2**).

1) When $C < \Gamma^*$, the two variants always disagree about the rate-limiting process and the values of V_c and A_n. This is a consequence of the fact that $(1 - \Gamma^*/C)$ is negative for $C < \Gamma^*$. For example, neglecting TPU, suppose that $W_c < W_j$ for $C < \Gamma^*$. In this case, $\min\{W_c, W_j\} = W_c$, so the min-*W* variant predicts Rubisco limitations with $V_c = W_c$ and $A_n = A_c$ (Figure **2a**). In contrast, the min-*A* variant uses the comparison $W_c \cdot (1 - \Gamma^*/C) > W_j \cdot (1 - \Gamma^*/C)$, and thus predicts RuBP regeneration limitations with $V_c = W_j$ and $A_n = A_j$ (Figure **2b**), leading to a discrepancy where the min-*A* variant predicts a larger V_c and smaller A_n (Figure **2c**). From this analysis, we can see that the relationship between A_c, A_j, A_p and A_n in the min-*W* variant is

$$A_n = \begin{cases} \max\{A_c, A_j\}, & C < \Gamma^* \\ \min\{A_c, A_j\} & \Gamma^* < C < \Gamma^* \cdot (1 + 3 \cdot \alpha_{old}) \\ \min\{A_c, A_j, A_p\}, & C \geq \Gamma^* \cdot (1 + 3 \cdot \alpha_{old}) \end{cases} \quad (\mathbf{3})$$

rather than Equation **2d**. Typical values of Γ^* are close to 40 µbar (approximately 40 µmol mol^{-1} or 40 ppm at typical atmospheric pressure), so this discrepancy between the variants only occurs at low values of C. Historically, such low values of C have been rarely accessed in gas exchange measurements because the available equipment could not easily reach them, but modern instruments can achieve lower values and researchers are now more likely to

encounter $C < \Gamma^*$. As will be shown below, this small difference prevents the min-*A* variant from matching measured CO_2 response curves, and it can have a large influence on parameter estimation (Section **3.5**).

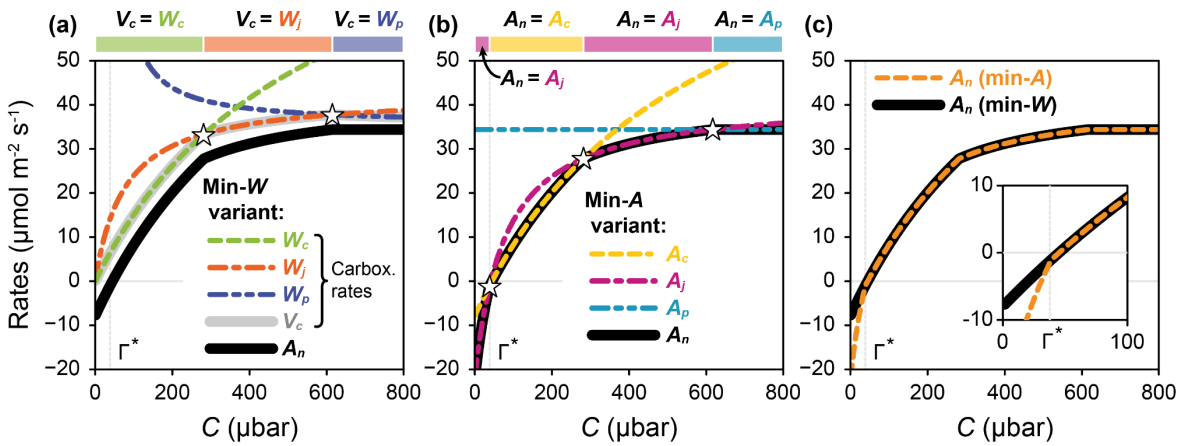

*Figure **2**: Comparison of outputs from the min-W and min-A variants for identical input parameter values with α_{old} = 0. (**a,b**) A_n (thick solid lines) as determined from potential carboxylation or assimilation rates (dashed lines) using Equations **1** and **2**, respectively. Crossover points where the rate-limiting process changes are marked with white stars. Solid rectangles indicate ranges of C where carboxylation or assimilation is limited by Rubisco, RuBP regeneration, or TPU. (**c**) Direct comparison of the variants across a range of C values. Inset: close-up showing the difference between the variants when $C < \Gamma^*$. All parameters were set to the values specified in Table **1**.*

Irrespective of any practical consequences, the min-*A* variant is not logically consistent because choosing the smallest net assimilation rate can lead to paradoxical results. For example, if V_{cmax} were to become zero when $C < \Gamma^*$ due to substantial Rubisco deactivation (Section **3.4**), the min-*A* variant would nevertheless predict $V_c = W_j$ and $A_n = A_j$, as discussed above. Assuming a nonzero J, this is a contradictory prediction that $V_c > 0$ when $V_{cmax} = 0$. In contrast, choosing a minimal carboxylation rate always produces self-consistent results.

2) The two variants always disagree about the number of points where the rate-limiting process changes; these special values of C are called crossover points. In the min-*A* variant, $A_c = A_j = -R_L$ when $C = \Gamma^*$ (Equations **2a** and **2b**), so a crossover point always exists at $C = \Gamma^*$ (Figure **2b**). However, in the min-*W* variant, W_c and W_j are generally not equal for $C = \Gamma^*$ (Equations **1a** and **1b**), so a crossover point does not always exist at $C = \Gamma^*$ (Figure **2a**). In other words, there is a spurious crossover point at $C = \Gamma^*$ in the min-*A* variant. This spurious crossover point

has been noticed before (Dubois et al., 2007; Gu et al., 2010) and the FRL modification has been used to address this issue, although this modification does not fully reconcile the variants in all situations (Section **3.2**). Note that these discrepancies between the min-*W* and min-*A* approaches persist in the 3-α version of the FvCB model, where they appear for $C < \Gamma^* \cdot (1 - \alpha_G + 2 \cdot \alpha_T)$ (Supplemental Section **S1.2**).

3.2. Rubisco Activity Does Not Always Limit Carboxylation at Low CO_2 Concentrations

Some fitting tools that implement the min-*A* variant introduce a constraint in their code where $A_n = A_c$ is enforced for $C \leq \Gamma^*$ (or possibly below another threshold value), even when Equation **2d** would predict otherwise (Figure **1** and Supplemental Section **S2.4**). Although rarely written explicitly as an equation, this is equivalent to replacing Equation **2d** with

$$A_n = \begin{cases} A_c, & C \leq \Gamma^* \\ \min\{A_c, A_j, A_p\}, & C > \Gamma^* \end{cases}$$

We refer to this as the "forced Rubisco limitation" (FRL) modification, and such variants as min-*A*+FRL variants. These variants agree with the min-*W* variant in situations where carboxylation is Rubisco limited for $C \leq \Gamma^*$.

However, the FRL modification will never be truly successful at fixing the min-*A* variant because there are no simple rules governing the progression of rate-limiting processes as C increases. Carboxylation can be limited by Rubisco activity or RuBP regeneration at low C, and a crossover between limitations is not guaranteed. Neglecting TPU, it is possible to analytically determine which process is limiting carboxylation at $C = 0$ and whether a crossover occurs (Supplemental Section **S3**). This process can be performed for many different values of $V_{c,max}$ and J, producing a map that shows where each possible sequence of assimilation rates occurs in the min-*W* variant (Figure **3a**). When including TPU, it is more straightforward to simulate a CO_2 response curve and extract the observed sequence of limitations; again, this can be performed for many values of $V_{c,max}$ and J, producing a map (Figure **3b**).

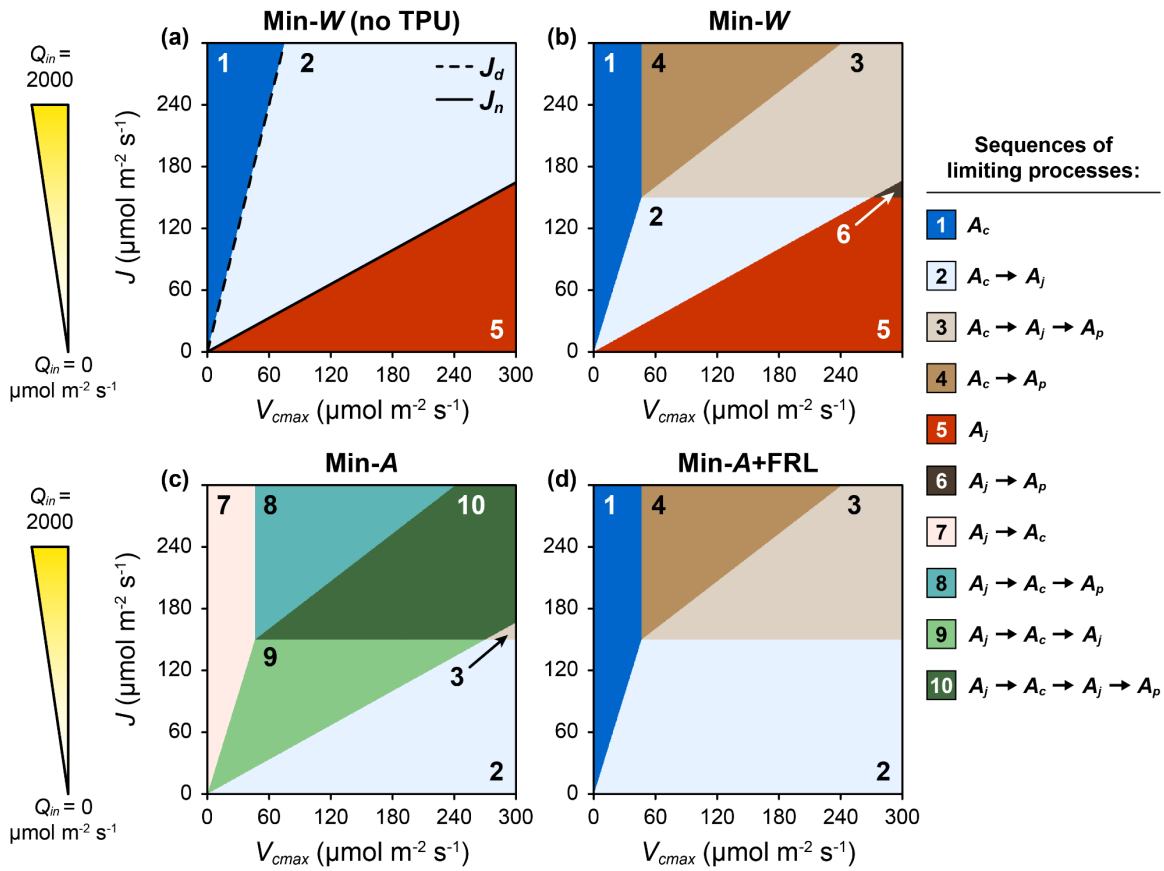

*Figure **3**: Predicted sequences of limiting processes as C increases from zero. (**a-d**) Maps of $(V_{c,max}, J)$-space, where labels within each region indicate the sequences as calculated by the min-W variant (neglecting or including TPU) (**a-b**), the min-A variant (**c**), or the min-A+FRL variant (**d**). The triangles to the left of (**a**) and (**c**) indicate an approximate relation between J and Q_{in}. Dashed and solid black lines in (**a**) show J_d and J_n (Equations **A6** and **A7** in Supplemental Section **S3**). All labels in (**b-d**) refer to observed sequences below a threshold of 2000 µbar. All parameters other than $V_{c,max}$ and J were set to the values specified in Table **1**.*

This analysis shows that when $V_{c,max}$ is relatively small compared to J, the min-*W* variant predicts Rubisco limitations for all values of C (dark blue regions labeled "1" in Figure **3**). This has been observed in modified tobacco with reduced Rubisco content (von Caemmerer et al., 1994), and this situation could potentially occur in plants under nitrogen stress (leading to low $V_{c,max}$) or in leaves exposed to high incident light levels (leading to high J). Likewise, when J is relatively small compared to $V_{c,max}$, the min-*W* variant predicts RuBP regeneration limitations for all values of C (red regions labeled "5" in Figure **3**). This situation could potentially occur in leaves exposed to low incident light levels (leading to low J), although this may be difficult to observe in practice due to a concurrent reduction in $V_{c,max}$ that tends to occur at low Q_{in}

(Lochocki et al., 2025; Sage et al., 2002; Taylor et al., 2022). Actual values of Q_{in} corresponding to high or low J depend strongly on details of leaf biochemistry and growth environment, but for many plants, $Q_{in} \leq 100$ µmol m^{-2} s^{-1} would correspond to low J while $Q_{in} \geq 1800$ µmol m^{-2} s^{-1} would correspond to high J. The maps also show that $A_c \rightarrow A_j \rightarrow A_p$ is not the only predicted sequence involving TPU limitations. In fact, a transition directly from Rubisco limited to TPU limited carboxylation ($A_c \rightarrow A_p$) can be observed in plants grown in low-light conditions (Sharkey, 2019). Note that there is no region corresponding to $A_j \rightarrow A_c$, indicating that this transition is not predicted to occur for typical parameter values (Supplemental Sections **S3** and **S4**).

Similar maps generated using the min-*A* and min-*A*+FRL variants show large differences relative to the min-*W* map (Figures **3c** and **3d**). Because of the spurious crossover point at Γ^* in the min-*A* variant (Section **3.1**), each region of the min-*A* map has one extra step compared to its min-*W* analog, several of which do not occur in the min-*W* map. For example, the $A_c \rightarrow A_p$ region of the min-*W* map (dark tan region labeled "4" in Figure **3b**) becomes an $A_j \rightarrow A_c \rightarrow A_p$ region in the min-*A* map (teal region labeled "8" in Figure **3c**). Because the min-*A*+FRL variant enforces Rubisco-limited assimilation at low C, its map lacks several sequences that are present in the min-*W* map. For example, the A_j region of the min-*W* map becomes an $A_c \rightarrow A_j$ region in the min-*A*+FRL map. These results demonstrate that the min-*W* and min-*A* variants do not predict the same transitions between limiting processes, and that the FRL modification does not fully bring the min-*A* variant into agreement with the min-*W* variant.

3.3. TPU Can Only Limit Carboxylation When Photosynthesis and Photorespiration Are Net Consumers of Free Inorganic Phosphate

Additional differences between the min-*W* and min-*A* variants can appear when $\alpha_{old} > 0$. This parameter is related to TPU and appears in Equations **1c** and **2c**. In the min-*W* variant, nonzero α_{old} introduces a downward slope to W_p (Figure **4a**). The resulting decrease in A_p with increasing C, termed "reverse sensitivity," is an identifying signature of TPU limitations, and the inclusion of α_{old} is essential to fit CO_2 response curves exhibiting reverse sensitivity (Busch et al., 2018; Harley and Sharkey, 1991). In the min-*A* variant, nonzero α_{old} similarly introduces a

downward slope to A_p at high values of C, but also produces divergent behavior at lower values of C (Figure **4b**). Mathematically, this behavior occurs because the denominator of Equation **2c** becomes zero when $C = \Gamma^* \cdot (1 + 3 \cdot \alpha_{old})$, and A_p approaches $-\infty$ as C approaches $\Gamma^* \cdot (1 + 3 \cdot \alpha_{old})$ from below. This issue does not occur for W_p because Equation **1c** sets W_p to ∞ for $C \leq \Gamma^* \cdot (1 + 3 \cdot \alpha_{old})$; however, it will occur if this condition is omitted from Equation **1c**.

Some fitting tools introduce a constraint in their code where TPU cannot set the net CO_2 assimilation rate below a fixed threshold value of C, which is often chosen to be 400 µbar (Supplemental Section **S2.4**). Although rarely written explicitly as an equation, when using the min-*A* variant this is equivalent to replacing Equation **2c** with

$$A_p = \begin{cases} \infty, & C \leq 400\ \mu\text{bar} \\ \frac{3 \cdot (C - \Gamma^*) \cdot T_p}{C - \Gamma^* \cdot (1 + 3 \cdot \alpha_{old})} - R_L, & C > 400\ \mu\text{bar} \end{cases}$$

or when using the min-*W* variant, replacing Equation **1c** with

$$W_p = \begin{cases} \infty, & C \leq 400\ \mu\text{bar} \\ \frac{3 \cdot C \cdot T_p}{C - \Gamma^* \cdot (1 + 3 \cdot \alpha_{old})}, & C > 400\ \mu\text{bar} \end{cases}$$

We refer to this as the "fixed TPU threshold" (FTT) modification, and such variants as the min-*A*+FTT or min-*W*+FTT variants. (Note that the min-*A*+FTT and min-*A*+FRL variants can be combined to form another variant with both types of modifications: the min-*A*+FRL+FTT variant.) These FTT variants agree with the min-*W* variant in situations where W_p is not the smallest carboxylation rate below the threshold value of C. However, if the min-*W* variant predicts $A_n = A_p$ for $\Gamma^* \cdot (1 + 3 \cdot \alpha_{old}) < C <$ 400 µbar, then the min-*W*+FTT and min-*A*+FTT variants will predict $A_n \neq A_p$ in that range, and then suddenly drop down to $A_n = A_p$ above the threshold (Figure **4c**). TPU limitations below 400 µbar are rare, but have been observed (Harley and Sharkey, 1991). Another potential issue with the FTT modification is that the divergent behavior of A_p will persist if the fixed threshold value is smaller than $\Gamma^* \cdot (1 + 3 \cdot \alpha_{old})$.

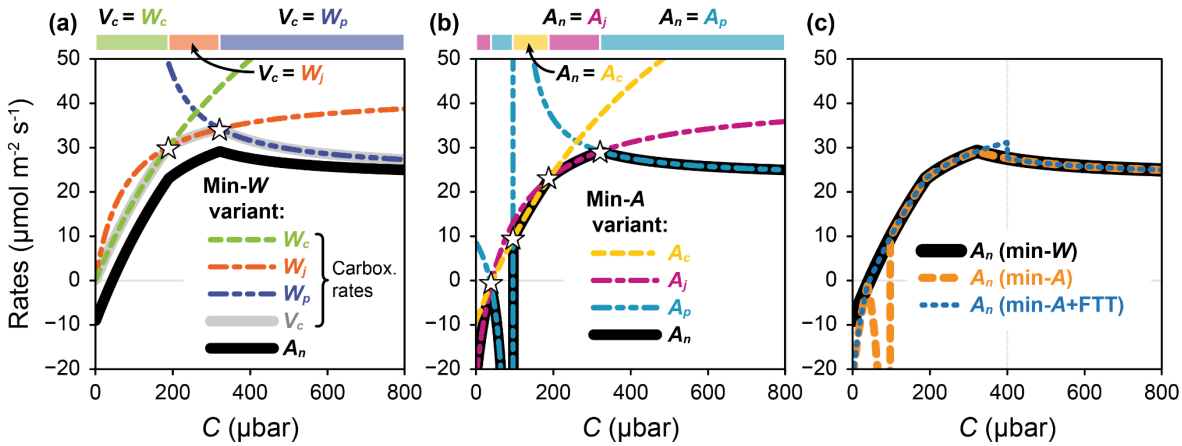

*Figure **4**: Comparison of min-W, min-A, and min-A+FTT variant outputs for identical input parameter values with $\alpha_{old} > 0$. (**a,b**) A_n (thick solid lines) as determined from potential carboxylation or assimilation rates (dashed lines) using Equations **1** and **2**, respectively. Crossover points where the rate-limiting process changes are marked with white stars. Solid rectangles indicate ranges of C where carboxylation or assimilation is limited by Rubisco, RuBP regeneration, or TPU. (**c**) Direct comparison of the variants across a range of C values. The following parameter values were used for these calculations: $V_{c,max}$ = 120 μmol m^{-2} s^{-1}, T_p = 8 μmol m^{-2} s^{-1}, and α_{old} = 0.5. All other parameters were set to the values specified in Table **1**.*

The FTT modification will never be truly successful at fixing the issues with Equation **2c** because it does not account for an important biochemical aspect of TPU limitations: TPU can only limit carboxylation when the net effect of photosynthesis and photorespiration is to shrink the pool of free inorganic phosphate (P_i) in the chloroplast by incorporating it into organic compounds, a process referred to as P_i consumption. P_i is required to synthesize adenosine triphosphate (ATP) via photophosphorylation, which in turn is used to regenerate RuBP. To achieve sustained ATP synthesis and RuBP regeneration, the net rate of P_i consumption due to photosynthesis and photorespiration (R_{pc}) must be balanced by the rate at which P_i is returned to the chloroplast through the utilization of triose phosphate for sugar production (T_p); otherwise, the pool of P_i would become depleted (Harley and Sharkey, 1991; Sharkey, 1985; von Caemmerer, 2000). In other words,

$$T_p = R_{pc} \tag{4a}$$

when TPU limits carboxylation. This requirement can be used to derive Equation **1c**, where the key step in the derivation is to relate R_{pc} to the RuBP carboxylation rate. Here we show that the restriction $C > \Gamma^* \cdot (1 + 3 \cdot \alpha_{old})$ is a natural consequence of this derivation.

By considering the stoichiometry of the carboxylation and oxygenation cycles and allowing for an additional release of P_i during photorespiration due to glycolate carbon that remains in the cytosol, it can be shown that

$$R_{pc} = \frac{V_c}{3} - \frac{V_o}{6} - \frac{\alpha_{old} \cdot V_o}{2}, \tag{4b}$$

where V_o is the rate of RuBP oxygenation (Harley and Sharkey, 1991; von Caemmerer, 2000). Next, it can also be shown that V_o is related to V_c via $V_o = 2 \cdot \Gamma^* \cdot V_c / C$ (von Caemmerer, 2000), allowing us to eliminate V_o from Equation **4b**:

$$R_{pc} = \frac{V_c}{3 \cdot C} [C - \Gamma^* \cdot (1 + 3 \cdot \alpha_{old})]. \tag{4c}$$

Here it is essential to note that, first, when $C = \Gamma^* \cdot (1 + 3 \cdot \alpha_{old})$, the net rate of P_i consumption is zero. Second, for smaller values of C, R_{pc} is negative, indicating that photosynthesis and photorespiration are actually releasing P_i. In both of these situations, it is not possible for TPU to become a limiting factor because photosynthesis and photorespiration are not shrinking the pool of P_i in the chloroplast, and hence the return of P_i via TPU is not necessary to prevent P_i depletion.

Finally, when TPU limits the carboxylation rate, V_c is denoted by W_p; in this case, we can now use Equations **4a** and **4c** to express the requirement for TPU limitation as

$$T_p = R_{pc} = \frac{W_p}{3 \cdot C} [C - \Gamma^* \cdot (1 + 3 \cdot \alpha_{old})]. \tag{4d}$$

Solving Equation **4d** for W_p and remembering that photosynthesis and photorespiration only consume P_i when $C > \Gamma^* \cdot (1 + 3 \cdot \alpha_{old})$ yields Equation **1c**. This lower C threshold for TPU limitations is a consequence of leaf biochemistry and its inclusion is guaranteed to prevent numerical errors such as negative or undefined W_p, unlike the fixed threshold used in the FTT modification. Although this threshold could be included in Equation **2c** from the min-*A* variant as a conditional statement like the one in Equation **1c**, none of the studies in the literature survey (Supplemental Section **2**) take this approach. Furthermore, doing so would not address the other issues with the min-*A* variant (Sections **3.2**, **3.3**, and **3.5**). Note that in the 3-α version

of the model, the biochemically derived C threshold for TPU limitations becomes $\Gamma^* \cdot (1 - \alpha_G + 2 \cdot \alpha_T) \cdot (1 + 3 \cdot \alpha_G + 4 \cdot \alpha_S + 6 \cdot \alpha_T)$ (Supplemental Section **S1.2**).

3.4. The Min-W Variant Can Be Extended To Include Substantial Rubisco Deactivation and RuBP Depletion at Low CO_2 Concentrations but the Min-A Variant Cannot

Besides the processes explicitly included in Equations **1** and **2**, Rubisco deactivation and RuBP depletion may also influence net CO_2 assimilation rates. Rubisco deactivation can occur when a leaf is held under low CO_2 conditions or under low light, likely by increasing the fraction of decarbamylated Rubisco, and the result of this process can be modeled as a reduction in V_{cmax} (Lochocki et al., 2025; Taylor et al., 2022; Sage et al., 2002). The min-*W* and min-*A* variants make different predictions in the hypothetical extreme case of full Rubisco deactivation for $C < \Gamma^*$, where V_{cmax} would become zero. Assuming no other parameter values change, W_c would also become zero but W_j and W_p would remain positive, so the min-*W* variant would predict Rubisco limitations with $A_n = A_c = -R_L$ (Equation **1**). Yet, A_j would be less than $A_c = -R_L$, so the min-*A* variant would predict a different limiting process and a smaller value of A_n (Equation **2**). In other words, the min-*A* variant does not allow substantial Rubisco deactivation to limit net CO_2 assimilation at low C, even when no Rubisco sites are active.

Similarly, the min-*A* variant does not predict a change in A_n due to substantial RuBP depletion, which can occur when $C < \Gamma^*$ because RuBP cannot be regenerated in this range. RuBP regeneration depends not only on electron transport and the availability of P_i, but also on the supply of 3-phosphoglyceric acid (PGA) from photosynthesis and photorespiration, which is reduced to unbound RuBP in a multi-step enzymatic pathway (von Caemmerer, 2000). When $C < \Gamma^*$, the supply of carbon as PGA is insufficient to regenerate enough RuBP, eventually depleting the pool of unbound RuBP. This can be understood by considering the carbon stoichiometry of the reduction pathway, where Rubisco uses RuBP at a rate of $V_c + V_o$ and PGA is produced at a rate of $2V_c + 1.5V_o$ (von Caemmerer, 2000). RuBP and PGA are five- and three-carbon molecules, respectively, so the difference between carbon supply and demand (Δ_c) is

$$\Delta_c = 3 \cdot (2V_c + 1.5V_o) - 5 \cdot (V_c + V_o) = V_c \cdot \left(1 - \frac{\Gamma^*}{C}\right), \quad (\mathbf{5})$$

where $V_o = 2 \cdot \Gamma^* \cdot V_c/C$ has been used to simplify the final expression. There is a carbon surplus ($\Delta_c > 0$) for $C > \Gamma^*$, which is exported from the chloroplast as triose phosphates. Carbon supply and demand are exactly equal ($\Delta_c = 0$) when $C = \Gamma^*$, and there is a deficit ($\Delta_c < 0$) for $C < \Gamma^*$. In the latter case, continued Rubisco activity draws from the chloroplastic pool of unbound RuBP without replenishing it.

Modeling RuBP depletion caused by insufficient carbon supply is more complex than Rubisco deactivation because it does not simply alter the value of a parameter such as V_{cmax} or J. Although not traditionally considered as part of the FvCB model, here we include it in the min-*W* variant by adding a fourth potential limitation to Equation **1d**:

$$V_c = \min\{W_c, W_j, W_p, W_d\} \tag{6a}$$

where W_d is the carboxylation rate limited by RuBP depletion. W_d is taken to be zero when C has been held below Γ^* long enough for Rubisco activity to completely deplete the pool of unbound RuBP, and is otherwise assumed to not limit carboxylation. This can be described mathematically as

$$W_d = \begin{cases} 0, & C < \Gamma^* \text{ for a sufficiently long time} \\ \infty, & \text{otherwise} \end{cases} \tag{6b}$$

Equation **6b** is not precise and omits two key details – incomplete RuBP depletion can lead to a small but nonzero W_d at low C, and W_d should depend continuously on C, RuBP pool size, and time. Nevertheless, this simplistic equation is instructive for understanding long-term steady-state net CO_2 assimilation at low C. When substantial RuBP depletion limits carboxylation, $V_c = W_d$ and the corresponding net CO_2 assimilation rate (A_d) can be found with Equations **1a** and **6b**:

$$A_d = \begin{cases} -R_L, & C < \Gamma^* \text{ for a sufficiently long time} \\ \infty, & \text{otherwise} \end{cases} \tag{7a}$$

With this, RuBP depletion can also be incorporated into the min-*A* variant by adding a fourth potential assimilation rate to Equation **2d**:

$$A_n = \min\{A_c, A_j, A_p, A_d\}. \quad \textbf{(7b)}$$

Equations **6** and **7** make contradictory predictions for A_n when C is below Γ^* for enough time to ensure substantial RuBP depletion. Assuming otherwise typical model parameter values in this scenario, W_c, W_j, and W_p would each be positive, so $W_d = 0$ would always be the smallest carboxylation rate, and the min-*W* variant would predict RuBP depletion limitations with $A_n = A_d = -R_L$ (Equation **6**). Conversely, A_c and A_j would each be smaller than $-R_L$, so the min-*A* variant would never predict $A_n = A_d$. In fact, Equation **7** would always predict the same rate and limiting process as Equation **2**. In other words, the min-*W* variant predicts a shift of A_n to $A_d = -R_L$ when substantial RuBP depletion occurs at low CO_2 concentrations, while the min-*A* variant does not allow substantial RuBP depletion to limit net CO_2 assimilation.

3.5. Comparing Both Variants to Measured CO_2 Response Curves

Since the min-*W* and min-*A* variants make different predictions for $C < \Gamma^*$, even when considering substantial Rubisco deactivation and RuBP depletion, it is possible to test them against measurements to determine which variant better represents reality. To do this, thirty-six CO_2 response curves were measured from *Nicotiana tabacum* (tobacco) cv. Samsun leaves at multiple incident light intensities using Licor LI-6800 portable gas exchange systems (Supplemental Section **S5.1**). Reference CO_2 concentration set-points ranging from 10 – 1800 µmol mol^{-1} were used, where the lowest values ensured several points in each curve with $C < \Gamma^*$. Each curve was fit with the *PhotoGEA* R package (Lochocki, 2025; Lochocki et al., 2025) on a C_i basis (i.e., by setting $C = C_i$) using tobacco temperature response parameters (Sharkey et al., 2007) and allowing $V_{c,max}$, J, R_L, T_p, and α_{old} to vary. *PhotoGEA* uses Equation **1** by default, but can optionally use Equations **2** or **6** instead, and can also optionally apply the FRL or FTT modifications. The fits were performed in four ways:

- min-*W variant (all C_i)*: The entire curve was fit twice using Equations **1** and **6**, and the result with smaller root mean square error (RMSE) was chosen as the best fit. If Equation **6** produced the best fit, the curve was considered to exhibit A_d limitations; otherwise, the curve was not considered to exhibit A_d limitations.

- min-*A+FTT variant (all C_i)*: The entire curve was fit using Equation **2** with a fixed TPU threshold of 400 µbar. There is no need for an additional fit using Equation **7** because Equations **2** and **7** make identical predictions.
- min-*W variant (C_i > 45 µbar)*: Points from the curve where C_i is above 45 µbar were fit using Equation **1**. Requiring C_i > 45 µbar ensured that no points with $C < \Gamma^*$ were used for the fit, since tobacco Γ^* is approximately 39 µbar at the measurement temperature of 27 °C.
- min-*A+FTT variant (C_i > 45 µbar)*: Points from the curve where C_i is above 45 µbar were fit using Equation **2** with a fixed TPU threshold of 400 µbar.

Note that the min-*W* variant predicts $A_n = -R_L$ when either substantial Rubisco deactivation or RuBP depletion limits net CO_2 assimilation for $C < \Gamma^*$ (Section **3.4**), so it is not possible to unambiguously attribute an observed A_d limitation to either process. Because of this, we consider W_d and A_d to represent both processes in the context of curve fitting. Also note that the min-*A*+FTT variant is used for these comparisons because the divergent behavior of the min-*A* variant with nonzero α_{old} severely interferes with the fitting process (Section **3.3**).

For a curve without such A_d limitations, an extrapolation of the fit made using the min-*W* variant for points where C_i is above 45 µbar agrees well with the measured points at lower C_i (Figure **5a**), suggesting that a good fit across all measured points could be achieved using Equation **1**. However, an extrapolation of the fit made using the min-*A*+FTT variant greatly diverges from the measured assimilation rates for C_i below 45 µbar, even though the two fits are identical for higher C_i (Figure **5b**). For a curve with A_d limitations, a similar extrapolation of the min-*W* fit made using points where C_i is above 45 µbar does not match the measured points at lower C_i, but $A_d = -R_L$ does lie close to those points (Figure **5e**), suggesting that a good fit across all measured points could be achieved using Equation **6**. An extrapolation of the min-*A*+FTT fit is even further from the measured points where C_i is below 45 µbar (Figure **5f**), but the min-*A* variant never predicts $A_n = A_d$, so a good fit across all C_i is unlikely.

As expected from these extrapolations, the min-*W* variant is able to closely match the measured points in each curve when fitting the entire range of C_i (Figures **5c** and **5g**), while the

min-*A*+FTT variant is not (Figures **5d** and **5h**). This is reflected in the RMSE values, where a lower RMSE indicates a better fit. The RMSE values of the min-*W* fits barely increase when adding the points with C_i < 45 µbar (0.140 vs. 0.160 for the curve without A_d limitations and 0.156 vs. 0.185 for the curve with A_d limitations), while there is a large increase in the min-*A*+FTT RMSE values (0.140 vs. 0.728 for the curve without A_d limitations and 0.156 vs. 1.312 for the curve with A_d limitations) (Figure **5**).

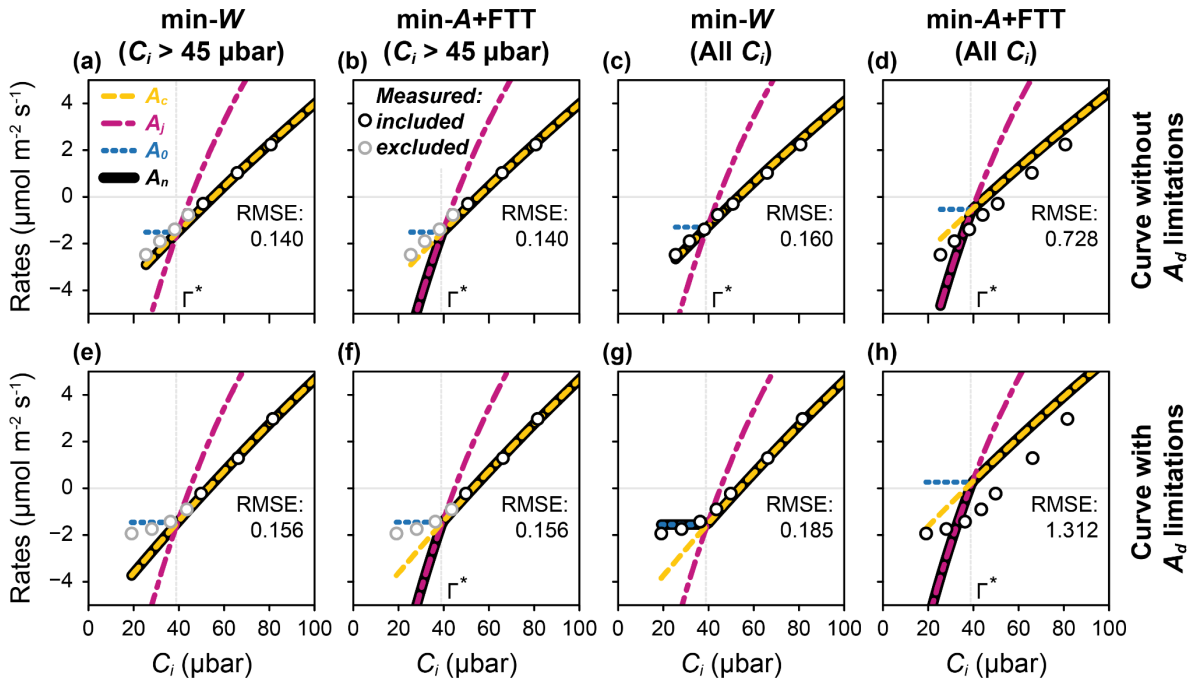

*Figure 5: Testing FvCB model variants against measured CO_2 response curves. Fits are shown for one curve without A_d limitations (**a-d**) and one with A_d limitations (**e-h**), both of which were measured with Q_{in} = 600 µmol m^{-2} s^{-1}. Fits were made using the min-W (**a,c,e,g**) or min-A+FTT variant (**b,d,f,h**), either limited to C_i above 45 µbar (**a,b,e,f**) or using all measured points (**c,d,g,h**). In each panel, measured points that were included in or excluded from the fit are shown as open black and gray circles, respectively. RMSE values are calculated from only the points included in each fit. A zoomed-in portion of each curve is shown to highlight differences at low C_i; see Supplemental Section **S5** for expanded views showing the fits across the entire range of measured C_i.*

These results hold across the entire set of thirty-six curves, where eighteen were found to exhibit A_d limitations at low C_i (Figure **6**). When fitting points at all C_i, the min-*A*+FTT variant generally produces larger RMSE values than the min-*W* variant, especially for curves that exhibit A_d limitations (Figure **6a**). Across all curves, the mean RMSE for the min-*W* fits is 0.32 µmol m^{-2} s^{-1}, while the mean RMSE for the min-*A*+FTT fits is more than twice as large at 0.79 µmol m^{-2} s^{-1} (see also Supplemental Figure **S10**). Fits made with the min-*W* variant have similar

RMSE values when including or excluding the points where C_i is below 45 µbar, but fits made with the min-*A*+FTT variant are appreciably worse when including points where C_i is below 45 µbar, even for curves that do not exhibit A_d limitations. Overall, this indicates that the min-*W* variant is able to represent leaf net CO_2 assimilation across all C_i values when potential limitations due to Rubisco deactivation and RuBP depletion are considered for $C < \Gamma^*$ (Equation **6**), while the min-*A*+FTT variant cannot.

Because the min-*A*+FTT variant does not closely match the observed values of A_n for $C < \Gamma^*$, parameter values estimated using this variant are greatly influenced by including points where C_i is below 45 µbar (Figures **6b-c**). As compared to fits made with the min-*W* variant, the min-*A*+FTT variant tends to underestimate both V_{cmax} and J. Values of V_{cmax} from min-*A*+FTT fits can be as much as 12 µmol m^{-2} s^{-1} lower (as much as 23% lower on a relative basis), while values of J can be as much as 17 µmol m^{-2} s^{-1} lower (as much as 12% lower on a relative basis).

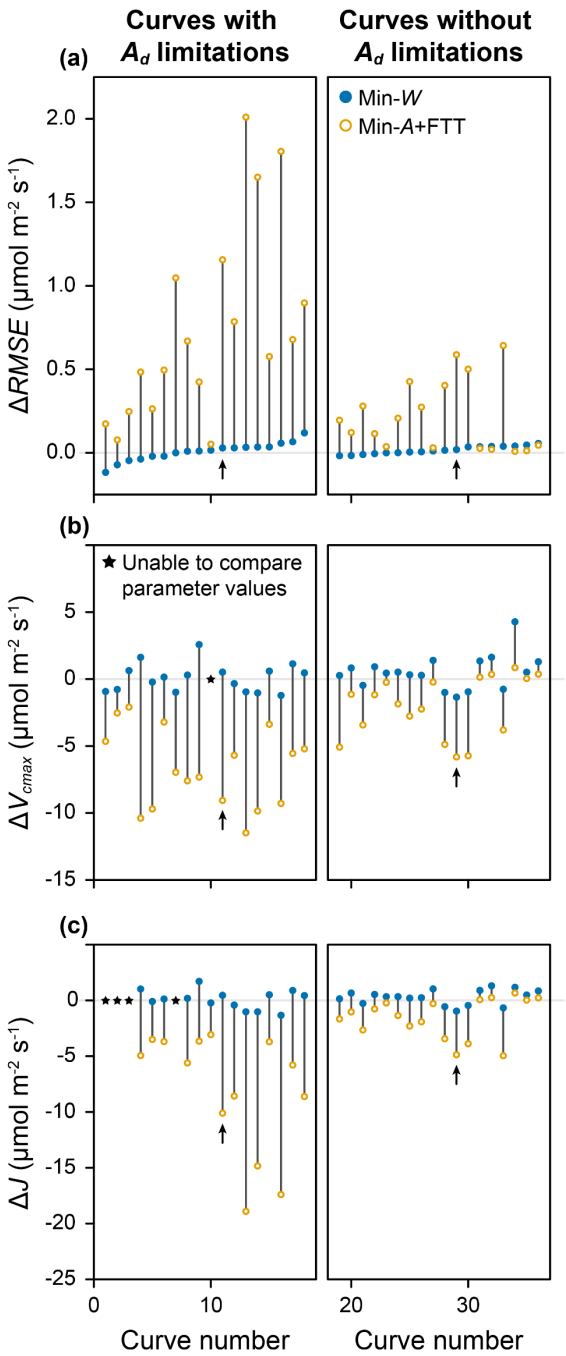

*Figure 6: Comparing fit results from thirty-six CO_2 response curves. Differences in (**a**) RMSE, (**b**) V_{cmax}, and (**c**) J that occur when including all points in the fit as compared to only using points where C_i is above 45 μbar, where $\Delta RMSE = RMSE^{All\ C_i} - RMSE^{C_i>45}$, $\Delta V_{cmax} = V_{cmax}^{All\ C_i} - V_{cmax}^{C_i>45}$, $\Delta J = J^{All\ C_i} - J^{C_i>45}$, and superscripts indicate which points were fit. Values from min-W and min-A+FTT variant fits are shown as filled blue circles and open yellow circles, respectively. Vertical gray lines connect the values from each variant for each curve. Results from curves that exhibit or do not exhibit A_d limitations are shown in the left and right columns, respectively. Some parameter values could not be reliably estimated from some curves; such parameters are marked with black stars. The two curves shown in Figure **5** are marked with black arrows.*

4. Discussion

The broad goal of this study was to summarize the most commonly used variants of the FvCB model and to compare them using mathematical and experimental approaches, providing what we hope is a useful resource for those learning the history of the development of this model. We also uncovered some issues with several of these variants and indicated the problems they can pose for FvCB model results and their interpretation. First, we showed that the min-*W* and the min-*A* variants disagree about the value of A_n and the rate-limiting process whenever $C < \Gamma^*$ (Section **3.1**). The FRL modification can address this discrepancy in some situations but does not fully reconcile the two variants (Section **3.2**). Second, we demonstrated that unrealistic predictions can occur when the biochemically-derived lower C threshold for TPU limitations, $\Gamma^* \cdot (1 + 3 \cdot \alpha_{old})$, is not included in the equations, or when a fixed threshold is used instead (Section **3.3**). Third, we showed that substantial Rubisco deactivation and RuBP depletion can be included in the min-*W* variant, but that the min-*A* variant cannot accommodate these processes for $C < \Gamma^*$ (Section **3.4**). Finally, we demonstrated that these issues prevent the min-*A*+FTT variant from closely fitting measured CO_2 response curves that include points where $C < \Gamma^*$, a potential source of error when estimating FvCB parameter values (Section **3.5**).

Half of the curves fit in this study exhibited signs of substantial Rubisco deactivation or RuBP depletion for $C < \Gamma^*$, requiring Equation **6** rather than Equation **1** to achieve a good fit. At present, it is not possible to predict whether a particular leaf will exhibit A_d limitations, making Equations **1** and **6** useful for describing curves but not necessarily for simulating assimilation rates when $C < \Gamma^*$. It is likely that the simplistic treatment of Rubisco deactivation and RuBP depletion in Equation **6** can be improved, enabling predictive abilities and producing even better agreement with measurements. Yet, because the min-*A* variant never allows these processes to limit assimilation at low C, it is unlikely to ever agree with the measured curves.

Parameter estimation from experimentally measured CO_2 response curves is a major application of the FvCB model. Whenever a curve fitting tool uses the min-*A*, min-*A*+FRL, or min-*A*+FTT variants rather than the min-*W* variant, there is a potential for errors in the estimated parameter values. These errors can occur whenever any of the points along the

curve are measured in conditions where the min-*W* variant disagrees with the other variants. This is likely to happen in the following situations:

- If the curve extends to low CO_2 concentrations (C roughly below 40 µbar), some of the measured points may satisfy $C < \Gamma^*$, and the min-*A* variant will assign the wrong limiting process in this range (Section **3.1**). This issue persists even when considering substantial Rubisco deactivation and RuBP depletion (Section **3.4**).
- If the curve extends to low CO_2 concentrations and was measured with low light levels around Q_{in} = 100 µmol m^{-2} s^{-1} (such that assimilation is limited by RuBP regeneration across the entire measured range), then the min-*A* variant will predict a sensitivity of the fit to $V_{c,max}$, even though $V_{c,max}$ would have no influence on the fit using the min-*W* variant. This error will persist even when adding the FRL modification (Section **3.2**).
- If the curve exhibits strong TPU limitations with reverse sensitivity, a nonzero value of α_{old} will be necessary. This will cause divergent behavior in the min-*A* variant at lower CO_2 concentrations, preventing a good fit (Section **3.3**).
- If the curve exhibits strong TPU limitations where $A_n = A_p$ for C below 400 µbar, the min-*A*+FTT variant will not be able to represent this behavior (Section **3.3**).

Here we show that estimates of J and $V_{c,max}$ made using the min-*A*+FTT variant are typically lower than those from the min-*W* variant, with underestimates exceeding 20%. Because the differences between the variants only appear for certain environmental conditions and plant characteristics, the only way to assess errors introduced by the min-*A* variant for a particular CO_2 response curve is to compare parameter estimates against those made using the min-*W* variant. Rather than attempting to quantify errors in a range of situations, it is simpler to always use the min-*W* variant.

Across the scientific literature, most CO_2 response curves are measured under high light and may contain only one or two points at very low CO_2 concentrations. It is also rare for TPU to be present for C below 400 µbar. Thus, the min-*A* variant is not likely to have caused significant errors in published work. It is also possible that some researchers intentionally avoid the complexities of fitting curves with points where $C < \Gamma^*$, either by only measuring points at

605 higher CO_2 set-points, or by excluding potentially problematic points (e.g., where $C_i < \Gamma^*$ or
606 $A_n < 0$) when fitting. Often this practice is not documented, even in recent comprehensive
607 guides to photosynthetic gas exchange measurements such as Busch et al. (2024), but it is likely
608 common enough to mitigate problems caused by the min-*A* approach. Nonetheless, the min-*A*
609 variant has no benefits over the min-*W* variant and is equally complex, leaving little reason for
610 its use. When it is desired to express the model equations using only assimilation rates, the
611 form presented in Equation **3** could be used instead.

612 As an argument against using the min-*A* variant despite the lack of current impact, the
613 likelihood of encountering some of these problematic situations may become larger as research
614 trends change and new research areas are formed. For example, a recently developed method
615 for estimating leaf cuticle conductance using gas exchange measurements actually necessitates
616 the measurement of CO_2 response curves under low irradiance (Márquez et al., 2022), a
617 situation where the min-*A* and min-*A*+FRL variants can produce incorrect parameter estimates.
618 The Laisk method for estimating C_i^* and R_L also requires low-light CO_2 response curves (Laisk,
619 1977; Walker and Ort, 2015). Efforts to improve crop yield and food security by engineering
620 plants with new Rubisco homologs may create situations where Rubisco-related parameters
621 like Γ^* and K_c take values significantly different from the ones in Table **1** (Amaral et al., 2024;
622 Carmo-Silva et al., 2015; Long et al., 2015; Parry et al., 2013). The most extreme situations may
623 occur in the field of astrobiology, where researchers study photosynthesis in hypothetical
624 extraterrestrial conditions with ambient gas environments and biochemical parameters that
625 may be very different from those found on Earth (Covone et al., 2021; Lehmer et al., 2021;
626 Lingam and Loeb, 2019; Mullan and Bais, 2018). It is therefore more important than ever for
627 plant scientists to clearly describe their curve fitting methods, including the equations used
628 (either min-*W* or min-*A*), whether any measured points satisfied $C < \Gamma^*$, and whether any
629 points at low C_i or A_n were excluded from fits.

630 A literature survey indicates that the min-*W* and min-*A* approaches have been used with
631 roughly equal frequency. Yet, the summarization and comparison of FvCB model variants
632 presented here indicates that the min-*W* approach, along with the biochemically-derived lower
633 threshold for TPU limitations, is the current state of the art, and likely the most appropriate

choice in many cases. Among min-*W* variants, the primary decision for researchers is to determine whether a situation calls for a version of the FvCB model that uses α_{old} (Equation **1**, the 1-α+BTT+min-*W*+NFL variant) or one that accounts for separate glycolate pathways via α_G, α_S, and α_T (Supplementary Equation **S1**, the 3-α+BTT+min-*W*+NFL variant).

Acknowledgements

The authors thank Stephen P. Long, Carl J. Bernacchi, Coralie E. Salesse-Smith, Yi Xiao, and Scott Rohde for helpful discussions.

This work was supported by Bill & Melinda Gates Agricultural Innovations grant investment ID 57248.

Any opinions, findings, and conclusions or recommendations expressed in this publication are those of the authors and do not necessarily reflect the views of the US Department of Agriculture. Mention of trade names or commercial products in this publication is solely for the purpose of providing specific information and does not imply recommendation or endorsement by the US Department of Agriculture. USDA is an equal opportunity provider and employer.

Competing Interests

The authors declare no competing interests.

Author Contributions

E.B.L. contributed to the conceptualization, modeling, data analysis and writing (original draft). J.M.M. contributed to conceptualization and revising the manuscript.

Data Availability

All data and R scripts for reproducing all analysis contained in this work are available online at https://github.com/ripeproject/FvCB-min-A.

Supporting Information

The supporting information includes Section **S1** (*Variations in FvCB Model Equations and Nomenclature*), Section **S2** (*Literature Survey*), Section **S3** (*CO_2 Response in the Min-W Variant*) Section **S4** (*Sequences of Limiting Processes for High Γ^* and/or Low K_c*), and Section **S5** (*Fitting Experimentally Measured CO_2 Response Curves*).

Works Cited

Amaral, J., Lobo, A.K.M., Carmo-Silva, E., 2024. Regulation of Rubisco activity in crops. New Phytologist 241, 35–51. https://doi.org/10.1111/nph.19369

Bellasio, C., Beerling, D.J., Griffiths, H., 2016. An Excel tool for deriving key photosynthetic parameters from combined gas exchange and chlorophyll fluorescence: theory and practice. Plant, Cell & Environment 39, 1180–1197. https://doi.org/10.1111/pce.12560

Bernacchi, C.J., Morgan, P.B., Ort, D.R., Long, S.P., 2005. The growth of soybean under free air [CO2] enrichment (FACE) stimulates photosynthesis while decreasing in vivo Rubisco capacity. Planta 220, 434–446. https://doi.org/10.1007/s00425-004-1320-8

Busch, F.A., 2020. Photorespiration in the context of Rubisco biochemistry, CO2 diffusion and metabolism. The Plant Journal 101, 919–939. https://doi.org/10.1111/tpj.14674

Busch, F.A., Ainsworth, E.A., Amtmann, A., Cavanagh, A.P., Driever, S.M., Ferguson, J.N., Kromdijk, J., Lawson, T., Leakey, A.D.B., Matthews, J.S.A., Meacham-Hensold, K., Vath, R.L., Vialet-Chabrand, S., Walker, B.J., Papanatsiou, M., 2024. A guide to photosynthetic gas exchange measurements: Fundamental principles, best practice and potential pitfalls. Plant, Cell & Environment 47, 3344–3364. https://doi.org/10.1111/pce.14815

Busch, F.A., Sage, R.F., 2017. The sensitivity of photosynthesis to O2 and CO2 concentration identifies strong Rubisco control above the thermal optimum. New Phytologist 213, 1036–1051. https://doi.org/10.1111/nph.14258

Busch, F.A., Sage, R.F., Farquhar, G.D., 2018. Plants increase CO2 uptake by assimilating nitrogen via the photorespiratory pathway. Nature Plants 4, 46–54. https://doi.org/10.1038/s41477-017-0065-x

Carmo-Silva, E., Scales, J.C., Madgwick, P.J., Parry, M. a. J., 2015. Optimizing Rubisco and its regulation for greater resource use efficiency. Plant, Cell & Environment 38, 1817–1832. https://doi.org/10.1111/pce.12425

Collatz, G.J., Ball, J.T., Grivet, C., Berry, J.A., 1991. Physiological and environmental regulation of stomatal conductance, photosynthesis and transpiration: a model that includes a laminar boundary layer. Agricultural and Forest Meteorology 54, 107–136. https://doi.org/10.1016/0168-1923(91)90002-8

Collatz, G.J., Berry, J.A., Farquhar, G.D., Pierce, J., 1990. The relationship between the Rubisco reaction mechanism and models of photosynthesis*. Plant, Cell & Environment 13, 219–225. https://doi.org/10.1111/j.1365-3040.1990.tb01306.x

Covone, G., Ienco, R.M., Cacciapuoti, L., Inno, L., 2021. Efficiency of the oxygenic photosynthesis on Earth-like planets in the habitable zone. Monthly Notices of the Royal Astronomical Society 505, 3329–3335. https://doi.org/10.1093/mnras/stab1357

De Souza, A.P., Wang, Y., Orr, D.J., Carmo-Silva, E., Long, S.P., 2020. Photosynthesis across African cassava germplasm is limited by Rubisco and mesophyll conductance at steady state, but by stomatal conductance in fluctuating light. New Phytologist 225, 2498–2512. https://doi.org/10.1111/nph.16142

Dubois, J.-J.B., Fiscus, E.L., Booker, F.L., Flowers, M.D., Reid, C.D., 2007. Optimizing the statistical estimation of the parameters of the Farquhar–von Caemmerer–Berry model

of photosynthesis. New Phytologist 176, 402–414. https://doi.org/10.1111/j.1469-8137.2007.02182.x

Duursma, R.A., 2015. Plantecophys - An R Package for Analysing and Modelling Leaf Gas Exchange Data. PLOS ONE 10, e0143346. https://doi.org/10.1371/journal.pone.0143346

Farquhar, G.D., von Caemmerer, S., 1982. Modelling of Photosynthetic Response to Environmental Conditions, in: Lange, O.L., Nobel, P.S., Osmond, C.B., Ziegler, H. (Eds.), Physiological Plant Ecology II: Water Relations and Carbon Assimilation, Encyclopedia of Plant Physiology. Springer, Berlin, Heidelberg, pp. 549–587. https://doi.org/10.1007/978-3-642-68150-9_17

Farquhar, G.D., von Caemmerer, S., Berry, J.A., 2001. Models of Photosynthesis. Plant Physiology 125, 42–45. https://doi.org/10.1104/pp.125.1.42

Farquhar, G.D., von Caemmerer, S., Berry, J.A., 1980. A biochemical model of photosynthetic CO2 assimilation in leaves of C3 species. Planta 149, 78–90. https://doi.org/10.1007/BF00386231

Gu, L., Pallardy, S.G., Tu, K., Law, B.E., Wullschleger, S.D., 2010. Reliable estimation of biochemical parameters from C3 leaf photosynthesis–intercellular carbon dioxide response curves. Plant, Cell & Environment 33, 1852–1874. https://doi.org/10.1111/j.1365-3040.2010.02192.x

Harley, P.C., Sharkey, T.D., 1991. An improved model of C3 photosynthesis at high CO2: Reversed O2 sensitivity explained by lack of glycerate reentry into the chloroplast. Photosynth Res 27, 169–178. https://doi.org/10.1007/BF00035838

He, Y., Matthews, M.L., 2023. Seasonal climate conditions impact the effectiveness of improving photosynthesis to increase soybean yield. Field Crops Research 296, 108907. https://doi.org/10.1016/j.fcr.2023.108907

Kirschbaum, M.U.F., Farquhar, G.D., 1984. Temperature Dependence of Whole-Leaf Photosynthesis in Eucalyptus pauciflora Sieb. Ex Spreng. Australian Journal of Plant Physiology 11, 519–538. https://doi.org/10.1071/pp9840519

Laisk, A.K., 1977. Kinetics of photosynthesis and photorespiration of C3 plants. Nauka.

Lehmer, O.R., Catling, D.C., Parenteau, M.N., Kiang, N.Y., Hoehler, T.M., 2021. The Peak Absorbance Wavelength of Photosynthetic Pigments Around Other Stars From Spectral Optimization. Frontiers in Astronomy and Space Sciences 8.

Lingam, M., Loeb, A., 2019. Photosynthesis on habitable planets around low-mass stars. Monthly Notices of the Royal Astronomical Society 485, 5924–5928. https://doi.org/10.1093/mnras/stz847

Lochocki, E.B., 2025. PhotoGEA: Photosynthetic Gas Exchange Analysis v1.2.0.

Lochocki, E.B., Salesse-Smith, C.E., McGrath, J.M., 2025. PhotoGEA: An R Package for Closer Fitting of Photosynthetic Gas Exchange Data With Non-Gaussian Confidence Interval Estimation. Plant, Cell & Environment 48, 5104–5119. https://doi.org/10.1111/pce.15501

Long, S.P., Marshall-Colon, A., Zhu, X.-G., 2015. Meeting the Global Food Demand of the Future by Engineering Crop Photosynthesis and Yield Potential. Cell 161, 56–66. https://doi.org/10.1016/j.cell.2015.03.019

Márquez, D.A., Stuart-Williams, H., Farquhar, G.D., Busch, F.A., 2022. Cuticular conductance of adaxial and abaxial leaf surfaces and its relation to minimum leaf surface conductance. New Phytologist 233, 156–168. https://doi.org/10.1111/nph.17588

Matthews, M.L., Marshall-Colón, A., McGrath, J.M., Lochocki, E.B., Long, S.P., 2022. Soybean-BioCro: a semi-mechanistic model of soybean growth. in silico Plants 4, diab032. https://doi.org/10.1093/insilicoplants/diab032

Moualeu-Ngangue, D.P., Chen, T.-W., Stützel, H., 2017. A new method to estimate photosynthetic parameters through net assimilation rate−intercellular space CO2 concentration (A−Ci) curve and chlorophyll fluorescence measurements. New Phytologist 213, 1543–1554. https://doi.org/10.1111/nph.14260

Mullan, D.J., Bais, H.P., 2018. Photosynthesis on a Planet Orbiting an M Dwarf: Enhanced Effectiveness during Flares. ApJ 865, 101. https://doi.org/10.3847/1538-4357/aadfd1

Parry, M.A.J., Andralojc, P.J., Scales, J.C., Salvucci, M.E., Carmo-Silva, A.E., Alonso, H., Whitney, S.M., 2013. Rubisco activity and regulation as targets for crop improvement. Journal of Experimental Botany 64, 717–730. https://doi.org/10.1093/jxb/ers336

Sage, R.F., Cen, Y.-P., Li, M., 2002. The activation state of Rubisco directly limits photosynthesis at low CO2 and low O2 partial pressures. Photosynthesis Research 71, 241–250. https://doi.org/10.1023/A:1015510005536

Sharkey, T.D., 2019. Is triose phosphate utilization important for understanding photosynthesis? Journal of Experimental Botany 70, 5521–5525. https://doi.org/10.1093/jxb/erz393

Sharkey, T.D., 1985. Photosynthesis in intact leaves of C3 plants: Physics, physiology and rate limitations. Bot. Rev 51, 53–105. https://doi.org/10.1007/BF02861058

Sharkey, T.D., Bernacchi, C.J., Farquhar, G.D., Singsaas, E.L., 2007. Fitting photosynthetic carbon dioxide response curves for C3 leaves. Plant, Cell & Environment 30, 1035–1040. https://doi.org/10.1111/j.1365-3040.2007.01710.x

Stinziano, J.R., Roback, C., Sargent, D., Murphy, B.K., Hudson, P.J., Muir, C.D., 2021. Principles of resilient coding for plant ecophysiologists. AoB PLANTS 13, plab059. https://doi.org/10.1093/aobpla/plab059

Taylor, S.H., Gonzalez-Escobar, E., Page, R., Parry, M.A.J., Long, S.P., Carmo-Silva, E., 2022. Faster than expected Rubisco deactivation in shade reduces cowpea photosynthetic potential in variable light conditions. Nat. Plants 1–7. https://doi.org/10.1038/s41477-021-01068-9

Von Caemmerer, S., 2013. Steady-state models of photosynthesis. Plant, Cell & Environment 36, 1617–1630. https://doi.org/10.1111/pce.12098

von Caemmerer, S., 2000. Biochemical Models of Leaf Photosynthesis. CSIRO Publishing. https://doi.org/10.1071/9780643103405

von Caemmerer, S., Evans, J.R., Hudson, G.S., Andrews, T.J., 1994. The kinetics of ribulose-1,5-bisphosphate carboxylase/oxygenase in vivo inferred from measurements of photosynthesis in leaves of transgenic tobacco. Planta 195, 88–97. https://doi.org/10.1007/BF00206296

Walker, A.P., Johnson, A.L., Rogers, A., Anderson, J., Bridges, R.A., Fisher, R.A., Lu, D., Ricciuto, D.M., Serbin, S.P., Ye, M., 2021. Multi-hypothesis comparison of Farquhar and Collatz photosynthesis models reveals the unexpected influence of empirical assumptions at

leaf and global scales. Global Change Biology 27, 804–822. https://doi.org/10.1111/gcb.15366

Walker, B.J., Ort, D.R., 2015. Improved method for measuring the apparent CO2 photocompensation point resolves the impact of multiple internal conductances to CO2 to net gas exchange. Plant, Cell & Environment 38, 2462–2474. https://doi.org/10.1111/pce.12562

Wang, Q., Chun, J.A., Fleisher, D., Reddy, V., Timlin, D., Resop, J., 2017. Parameter Estimation of the Farquhar—von Caemmerer—Berry Biochemical Model from Photosynthetic Carbon Dioxide Response Curves. Sustainability 9, 1288. https://doi.org/10.3390/su9071288

Wu, A., Brider, J., Busch, F.A., Chen, M., Chenu, K., Clarke, V.C., Collins, B., Ermakova, M., Evans, J.R., Farquhar, G.D., Forster, B., Furbank, R.T., Groszmann, M., Hernandez-Prieto, M.A., Long, B.M., Mclean, G., Potgieter, A., Price, G.D., Sharwood, R.E., Stower, M., van Oosterom, E., von Caemmerer, S., Whitney, S.M., Hammer, G.L., 2023. A cross-scale analysis to understand and quantify the effects of photosynthetic enhancement on crop growth and yield across environments. Plant, Cell & Environment 46, 23–44. https://doi.org/10.1111/pce.14453

Xiao, Y., Sloan, J., Hepworth, C., Osborne, C.P., Fleming, A.J., Chen, X., Zhu, X.-G., 2021. Estimating uncertainty: A Bayesian approach to modelling photosynthesis in C3 leaves. Plant, Cell & Environment 44, 1436–1450. https://doi.org/10.1111/pce.13995

Yin, X., Busch, F.A., Struik, P.C., Sharkey, T.D., 2021. Evolution of a biochemical model of steady-state photosynthesis. Plant, Cell & Environment 44, 2811–2837. https://doi.org/10.1111/pce.14070

Yin, X., Struik, P.C., 2017. Can increased leaf photosynthesis be converted into higher crop mass production? A simulation study for rice using the crop model GECROS. Journal of Experimental Botany 68, 2345–2360. https://doi.org/10.1093/jxb/erx085